Photochemical & Photobiological Sciences

Early photochemical events of a ruthenium(II) molecular dyad capable of performing photochemical water oxidation and of its model compounds

Journal:	*Photochemical & Photobiological Sciences*
Manuscript ID	PP-ART-11-2018-000530.R1
Article Type:	Paper
Date Submitted by the Author:	04-Feb-2019
Complete List of Authors:	Nastasi, Francesco; Universita degli Studi di Messina, Santoro, Antonio; University of Messina, Dipartimento di Science Chimiche Serroni, Scolastica; University of Messina, Department of Inorganic Chemistry, Analytical Chemistry, and Physical Chemistry Campagna, Sebastiano; Universita degli Studi di Messina, Scienze chimiche, biologiche, farmaceutiche ed ambientali Kaveevivitchai, Nattawut; University of Houston, Chemistry Thummel, Randolph; University of Houston, Chemistry

Early photophysical events of a ruthenium(II) molecular dyad capable of performing photochemical water oxidation and of its model compounds

Francesco Nastasi,[a,*] Antonio Santoro,[a] Scolastica Serroni,[a] Sebastiano Campagna,[a,*] Nattawut Kaveevivitchai[b] and Randolph P. Thummel.[b,*]

(a) Department of Chemical, Biological, Pharmaceutical and Environmental Sciences, University of Messina, and Centro Interuniversitario per la Conversione Chimica dell'Energia Solare (SOLARCHEM, sezione di Messina), 98166 Messina, Italy.

(b) Department of Chemistry, University of Houston, 122 Fleming Building, Houston, Texas, 77204-5003, USA.

Abstract

The early photophysical events occurring in the dinuclear metal complex [(ttb-terpy)(I)Ru(μ-dntpz)Ru(bpy)$_2$]$^{3+}$ (**2**; ttb-terpy = 4,4',4"-tri-tert-butyl-terpy; bpy = 2,2'-bipyridine; dntpz = 2,5-di-(1,8-dinaphthyrid-2-yl)pyrazine) - a species containing the chromophoric {(bpy)$_2$Ru(μ–dntpz)}$^{2+}$ subunit and the catalytic {(I)(ttb-terpy)Ru(μ–dntpz)}$^{+}$ unit, already reported to be able to perform photocatalytic water oxidation - have been studied by ultrafast pump-probe spectroscopy in acetonitrile solution. The model species [Ru(bpy)$_2$(dntpz)]$^{2+}$ (**1**), [(bpy)$_2$Ru(μ–dntpz)Ru(bpy)$_2$]$^{4+}$ (**3**), and [(ttb-terpy)(I)Ru((μ–dntpz)Ru[(ttb-terpy)(I)]$^{2+}$ (**4**) have also been studied. For completeness, the absorption spectra, redox behavior of **1-4** and the spectroelectrochemistry of the dinuclear species **2-4** have been investigated. The usual ^{3}MLCT (metal-to-ligand charge transfer) decay, characterized by relatively long lifetimes on the ns timescale, takes place in **1** and **3**, whose lowest-energy level involves a {(bpy)$_2$Ru(dntpz)}$^{2+}$ unit, whereas for **2** and **4**, whose lowest-energy excited state involves a ^{3}MLCT centered on the {(I)(ttb-terpy)Ru(μ–dntpz)}$^{+}$ subunit, the excited-state lifetimes are on the ps timescale, possibly involving population of a low-lying ^{3}MC (metal-centered) level. Compound **2** also exhibits a fast process, with a time constant of 170 fs, which is attributed to intercomponent energy transfer from the MLCT state centered in the {(bpy)$_2$Ru(μ–dntpz)}$^{2+}$ unit to the MLCT state involving the {(I)(ttb-terpy)Ru(μ–dntpz)}$^{+}$ unit. Both the intercomponent energy transfer and the MLCT-to-MC activation process take place from non-equilibrated MLCT states.

Introduction

Ruthenium polypyridine complexes have been extensively investigated as molecular water oxidation catalysts (WOCs).[1] Since the appearance more than 30 years ago of the first well-defined molecular WOC , the so-called "blue dimer", $[(bpy)_2(H_2O)Ru(\mu\text{-}O)Ru(H_2O)(bpy)_2]^{4+}$ (bpy = 2,2'-bipyridine),[2] an impressive number of WOCs based on Ru complexes have been prepared and studied, particularly in the last 10 years.[3] This line of research has led to the synthesis of some of the most efficient and fast water WOCs reported so far. These systems reach turnover frequencies (TOFs) comparable or even higher (200-1000 s^{-1}) than those of the natural water oxidation catalyst, the Mn_4CaO_5 cluster.[3a] Such studies have also helped to clarify the mechanism of water oxidation by Ru molecular catalysts, which are now classified according to two routes. One route is the water nucleophilic attack (WNA), in which a water molecule attacks the unstable, electron poor Ru^{V}=O of the WOC. The other route is the bimolecular, radical O-O coupling pathway (I2M), in which the O-O bond is formed between two Ru^{V}-oxo species with significant Ru^{IV}-oxyl radical character.[4,5]

Beside the development of new mononuclear Ru WOCs, multicomponent species containing a Ru chromophore unit and a Ru WOC have been prepared.[6,7] Such molecular dyads have also been anchored on surfaces (typically, mesoporous TiO_2) to play the role of the photoanode in dye-sensitized photoelectrochemical cells (DSPECs), allowing fast electron transfer from the WOC to the oxidixed chromophore, thus alleviating the problem of charge recombination.[8]

Whereas certain mechanistic studies have been performed, only a few of these studies have been focused on the early photophysical events that occur upon light excitation in Ru WOCs. One of the rare examples is the investigation, by ultrafast spectroscopic techniques, of the early photophysical events occurring in $[Ru(bpy)(terpy)(H_2O)]^{2+}$ and $[Ru(bpy)(terpy)(D_2O)]^{2+}$ (terpy = 2,2':6',2"-terpyridine).[9] This study revealed the impact of hydrogen-bond dynamics on nonradiative decay, via modification of the excited-state equilibration between metal-to-ligand charge-transfer (MLCT) and metal-centered (MC) triplet states.[9] Even rarer are ultrafast investigations of early

photophysical events occurring in molecular chromophore-catalyst dyad assemblies designed to perform water oxidation.

Here we report the pump-probe ultrafast transient absorption spectroscopy of the molecular dyad **2** (see **Figure 1**), consisting of a $Ru(bpy)_2(BL)$-type chromophore and of a Ru(terpy)(BL)(I)-type species which is considered a precursor of the $[Ru(terpy)(BL)(H_2O)]^{2+}$ WOC (since in aqueous solution, the halide ligand is replaced by a water molecule[10]). In the present case, the bridging ligand BL is 2,5-di-(1,8-dinaphthyrid-2-yl)pyrazine (dntpz), a bis-chelating bridging ligand. Compound **2**, whose general formula is $[(ttb\text{-}terpy)(I)Ru(\mu\text{-}dntpz)Ru(bpy)_2]^{3+}$ (ttb-terpy = 4,4',4''-tri-tert-butyl-terpy), has been demonstrated to couple the properties of the chromophoric and catalytic moieties, yelding molecular oxygen upon light excitation in aqueous solution, in the presence of sodium persulfate as the sacrificial oxidant.[7] The turnover number (TON) of such a system is 134 after 6 h of irradiation which is much higher than that obtained for a similar system containing the monomeric chromophore and analogous WOC.[7] For completeness, the present work also reports the transient absorption spectroscopy of the mononuclear chromophore species, **1**, and of the two symmetric dinuclear compounds **3** and **4** (structural formulae shown in **Figure 1**), together with their absorption spectra, redox behavior and spectroelectrochemical properties. The absorption and redox properties of **1** and **2**, as well as the redox properties of **3**, have already been partially reported[3d,11] and are shown and discussed here for comparison purposes.

We attempted to investigate the ultrafast spectroscopy of **2** and **4** also in the presence of sodium persulfate in aqueous solution, the conditions in which the photocatalysis takes place. However, despite several efforts using slightly different experimental conditions, the compounds were not stable under laser irradiation. We were therefore forced to limit our work to acetonitrile solution.

Results and Discussion

Absorption spectra. The aborption spectra of **1-4** in acetonitrile are shown in **Figure 2** and main data are collected in **Table 1**. The visible region is dominated by spin-allowed MLCT bands. In all the cases, the acceptor ligand of the lowest-energy MLCT transition is the dntpz ligand, which is easier to reduce than terpy or bpy (see redox data). The lowest energy MLCT band of **1** is significantly higher in energy (λmax = 543 nm) than those of the other compounds, since dntpz in **1** does not play the role of a bridging ligand, its π^* orbital is thus higher in energy than in **2-4**. In **1**, the band with a maximum at 424 nm is attributed to a Ru→bpy CT transition, and the bands in the UV region are dominated by ligand-centered (LC) bands (see **Table 1**). In **3**, as a consequence of double coordination of dntpz, the lowest energy MLCT absorption band moves to around 655 nm; it also appears to be vibrationally structured. The band at about 490 nm is probably a LC transition involving the bridging ligand (note that it appears at practically the same energy in **2** and **4**). The MLCT band is even more red-shifted in the symmetric compound **4** which shows λmax at wavelengths longer than 720 nm, as expected: the donor orbital of the MLCT transition, the dπ metal orbital(s), is actually at higher energy than in **2** because of the presence of the iodide ligands. The intense band at about 280 nm is typical of bpy-centered $\pi-\pi^*$ transitions, which are present in the absorption spectra of **1-3** and obviously absent in **4**.

The absorption spectrum of the asymmetric dinuclear species **2** is more complex, particularly as far as the lowest-energy MLCT transitions are concerned. The MLCT bands involving the peripheral ligands bpy and ttb-terpy are expected at shorter wavelenths than 520 nm and probably contribute to the absorption features between 400 and 550 nm, overlapped with the LC transition involving the bridging ligand. The region between 570 and 820 nm should be dominated by the MLCT transitions involving the bridging ligand, with the {(I)(ttb-terpy)Ru}→(μ-dntpz) CT transition at lower energy than the {$(bpy)_2$Ru}→(μ-dntpz) CT one, owing to the different electron density on the metal centers, also in agreement with the redox data (vide infra). In fact, the

low energy region of the spectrum of **2** has a maximum at about 695 nm, with two shoulders at 775 and 625 nm. A comparison between the spectra of **2, 3,** and **4** suggests that the two shoulders should correspond to the {(I)(ttb-terpy)Ru}→(μ-dntpz) CT and {$(bpy)_2$Ru}→(μ-dntpz) CT transitions, respectively, with the experimental maximum at 695 nm due to an overlap between the two low-energy MLCT bands. The absorption spectra of **2-4**, allows one to identify the various MLCT bands as belonging to specific subunits and supports a localized behavior of excited states.

Table 1. Absorption band maxima and main shoulders (visible region) and their assignments of **1-4** in acetonitrile. Only spin-allowed transitions are reported. For more details, see text.

Coumpound	λ /nm(ε/$M^{-1}cm^{-1}$)	Electronic transitions
1	424 (8000) 543 (6600)	{$(bpy)_2$Ru}→bpy CT {$(bpy)_2$Ru}→ dntpz CT
2	625 (6300) 695 (12600) 775(5400)	{$(bpy)_2$Ru}→(μ-dntpz) CT overlap of MLCT bands[a] {(I)(ttb-terpy)Ru}→(μ-dntpz) CT
3	490 (9800) 655 (14000)	LC (μ-dntpz) Ru→ dntpz CT
4	500 (23600) 720 (20000)	Ru→ ttb-terpy CT Ru→ dntpz CT

(a) This maximum is due to overlap between two MLCT transitions, see text.

Transient absorption spectroscopy. Pump-probe transient absorption spectroscopy of **1-4** has been studied in acetonitrile solution at room temperature, with an excitation wavelength of 400 nm. The transient absorption spectrum of the mononuclear species **1** is shown in **Figure 3**. The spectrum recorded immediately after the pump pulse (about 140 fs) is characterized by an intense absorption at λ < 540 nm, maximizing at about 490 nm, and a broad absorption at wavelengths longer than 580 nm, extending up to 780 nm, the limit of our experimental setup. The transient absorption spectrum contains a minimum, corresponding to the ground state absorption bleaching at about 550 nm. Significantly, the transient absorption feature, in particular the part at higher energy, further develops with a time constant of about 980 fs (**Figure 3, top**). In Ru(II) polypyridine complexes, intersystem crossing is known to occur on the 100 fs timescale or faster,[12] and internal

conversion between MLCT states at different energy levels within a single metal center is expected to occur on a similar timescale:[¶,13] As a consequence, the 980 fs time constant process can hardly be assigned to such processes. We propose that the fast decay process of **1** is due to a structural reorganization within the dnptz ligand such as enhanced planarization leading to increased delocalization of the promoted electron within the large ligand and enhanced absorption by the dntpz radical anion. A second decay process takes place in **1**, with a time constant of 250 ps (**Figure 3, middle panel)**, possibly due to vibrational cooling.[14] Finally the spectrum tends to monotonically decay to the ground state on much longer time scale than our apparatus. Such a behavior is expected since the emission lifetime of **1** (emission maximum at 807 nm[3d] under these experimental conditions) is probably longer than 10 ns, by comparison with other similar Ru(II) complexes emitting in the same spectral range.[15]

Compound **3** is the symmetric dinuclear analogue of **1** and exhibits a transient spectrum with bleaching of the lowest-energy MLCT band in the 600-680 nm region, and absorption features at $\lambda < 610$ nm and at $\lambda > 680$ nm (**Figure 4**). Even in **3** a fast process takes place, with a time constant of 1.6 ps, evidencing increased absorption below 520 nm and at wavelengths longer than 700 nm, and a moderate reduced absorption between 530 and 660 nm (**Figure 4, top**). In this case, we attribute the process to some increased delocalization of the promoted electron within the bridging ligand connected with structural modification. Vibrational cooling is successively occurring in 220 ps (**Figure 4, middle**), and decay to the ground state finally occurs (isosbestic points at $\lambda = 580$ and 680 nm with $\Delta A = 0$, see **Figure 4, bottom**) with a time constant of about 4.5 ns.

The symmetric dinuclear compound **4** contains two potential WOC subunits, which themselves are also strong light absorbers. The lowest-lying excited-state level of **4**, due to the simultaneous presence of a terpy and a halide ligand is expected to be a triplet MLCT state very close in energy to a triplet MC level, which promotes fast radiationless excited-state decay.[13,16] The transient absorption spectrum of **4** is shown in **Figure 5**. It exhibits bleaching of the ground state absorption due to the MLCT bands at about 500 and 730 nm. This is compatible with the MLCT

nature of the excited state that shows an intense transient absorption covering the whole visible region, peaking around 600 nm and possibly due to absorption of the bridging ligand radical anion. Another intense absorption is observed below 500 nm. The initial evolution of the transient spectrum shows the decrease of the visible region transient absorption in the range 520-750 nm, with a time constant of about 500 fs (**Figure 5, top**). In spite of the different shape of the transient spectrum of **4** with respect to that of **3**, the initial evolution of the two transient spectra are qualitatively similar, including an apparent isosbestic point in the 500-540 nm region. On this basis, we attribute the fast initial decay of **4** to charge redistribution within the dntpz radical anion, connected to some structural reorganization similar to **3**. After the initial process, the transient spectrum of **4** decays monotonically to the ground state with isosbestic points at λ about 550 and 545 nm with $\Delta A = 0$ (**Figure 5, bottom**) with a time constant of 28 ps. This process involves decay of the ^{3}MLCT state to the ground state probably via a thermally-activated process to the ^{3}MC level which funnels rapid radiationless decay. The relatively slow MLCT vibrational cooling process occurring in **1** and **3** (time constant 250 and 220 ps, respectively) is not present in **4** since it cannot compete with decay to the ground state assisted by the MC state.

The transient absorption spectrum of **2** is shown in **Figure 6**. Compound **2** is an asymmetric dinuclear species, containing two different chromophores with two different low-lying MLCT states, so energy transfer from the upper lying $\{(bpy)_2Ru\}\rightarrow$(μ-dntpz) CT level to the lower-lying $\{(I)(ttb\text{-}terpy)Ru\}\rightarrow$(μ-dntpz) CT state could be expected. This process is expected to be quite fast: indeed, similar down-hill energy transfer processes between nearby Ru(II) chromophores across the 2,3-bis(2-pyridyl)pyrazine (2,3-dpp), a bridging ligand related to dnptz, sharing a pyrazine ring between two metal centers), in polynuclear Ru/Os complexes take place with time constants of 100 fs or even faster.[17] Actually, such an energy transfer corresponds mainly to a metal-to-metal electron transfer, coupled to electron redistribution within the bridging ligand through a bridge which allows for a relatively significant electronic coupling (see redox section). Therefore, it can be foreseen that the above mentioned inter-component energy transfer in **2**, if visible, is close to the

limit of our equipment (140 fs)**.** The initial transient absorption spectrum of **2** (**Figure 6**) shows bleaching of the MLCT bands and transient absorption below 460 nm and between 520 and 650 nm, the typical range of the bridging ligand radical anion absorption, already shown by the other compounds of this series, and is mainly attributed to formation of the triplet MLCT state centered in the Ru(terpy)(μ–BL)(I) subunit, by comparison with the transient absorption spectrum of **4** (**Figure 5**). A quite fast decay process takes place, with a time constant of 170 fs (**Figure 6, top).** By analogy with **4**, this fast process could be assigned to charge redistribution within the dntpz radical anion coupled with some structural reorganization. However the time constant of the process seems to be too fast in comparison with that of **4**. Moreover, whereas the process in **4** does not show any change in the absorption spectrum shape in the 520-680 nm region, in **2** the apparently structured transient absorption loses the contribution around 530 nm, where the initial transient absorption spectrum of **3** has a peak (see **Figure 4, top panel).** The above arguments suggest that the 170 fs process mainly involves the expected very fast $\{(bpy)_2Ru\}\rightarrow$(μ-dntpz) CT to {(I)(ttb-terpy)Ru}→(μ-dntpz) CT energy transfer. The successive decay process (time constant, 2.5 ps) can be attributed to structural reorganization and charge redistribution within the bridging ligand. It can also be noted that the time constant of this process is also very close to that recorded for the equilibration between MLCT and MC states in $[Ru(bpy)(terpy)(H_2O)]^{2+}$ in aqueous solution (2 ps).[9] Such an excited-state equilibration can also contribute to the 2.5 ps decay of **2**. Finally, direct decay to the ground state occurs, with a time constant of ca. 25 ps (**Figure 6, bottom panel**). Even in **2**, as already noted for **4**, the relatively slow vibrational cooling process recorded in **1** and **3** cannot take place since it cannot compete with the MC-assisted decay to the ground state.

The time constants of the various excited-state decays of **1-4**, together with their attributions, are gathered in **Table 2.** From the above discussion, and also by a cursory look at **Table 2**, it appears that both the intercomponent energy transfer and the thermally-activated MLCT-to-MC processes take place on timescales that are much shorter than ^{3}MLCT vibrational cooling as evidenced by **1** and **3**, and therefore most likely involve non-equilibrated MLCT states.

Table 2. Time constants and relative attributions of the excited-state decays of **1-4** in acetonitrile. For more details, see text.

	1	**2**	**3**	**4**
energy transfer		170 ± 19 ps		
structural reorganization/charge redistribution within the reduced bridge	980 ± 97 fs	2.51 ± 0.66 ps[a]	1.63 ± 0.13 ps	478 ± 20 fs
vibrational cooling	250 ± 23 ps		220 ± 23 ps	
direct decay to the ground state	> 10 ns[b]	24.7 ± 1.2 ps	4.48 ± 0.94 ns	28.3 ± 3.9 ps

(a) This process could also include equilibration between MLCT and MC levels. (b) We cannot measure this decay, since the transient spectrum appears to be almost stable on the experimental limit. The extremely slow decay, however, indicates that 10 ns is a low limit for the time constant of the process.

Redox behavior and spectroelectrochemistry. The redox data of **1-4** are displayed in **Table 3**. The oxidation processes are mainly metal centered and the reduction processes are ligand centered, as usual for Ru(II) polypyridine complexes.

A cursory look at the data in **Table 3** makes it clear that the first two processes of the dinuclear compounds involve reduction of the bridging ligand, which is reduced twice before peripheral ligand reduction takes place, much like the dinuclear Ru(II) complexes involving the similar 2,3-dpp bridging ligand.[18]

First and second oxidation processes of the asymmetric dinuclear complex **2** are easily attributed to sequential oxidation of the {(I)(ttb-terpy)Ru}and {$(bpy)_2$Ru} subunits, respectively, slightly modified with respect to the corresponding processes in **3** and **4**. The difference in first and second oxidation potentials (ΔV) in the symmetric dinuclear compounds **3** and **4** is related to the comproportionation constant, in its turn related to the electronic interaction between the metal subunits mainly occurring via superexchange interaction across the bridging ligand.[19] For bridging ligands having relatively low-lying π^* orbitals, like dntpz, the dominant superexchange pathway is usually the electron-transfer route.[20] Since ΔV, which is proportional to the comproportional constant, is relatively similar in **3** and **4** (230 and 180 mV, respectively), the metal-metal electronic

interaction could seem similar in **3** and **4**, or even smaller in **4**, assuming Koopmans theorem as valid.[21] This conclusion, anyway, seems to be in disagreement with the general assumption that metal-metal interaction mediated by superexchange via an electron transfer pathway depends on the energy gap between metal orbitals and empty π* bridging ligand orbitals.[20] In fact, this energy gap is much larger for **3** than for **4** (1.65 V and 1.36 V, respectively, roughly estimated by the difference in the first oxidation and first reduction processes, see data in **Table 3**), as a direct consequence of the fact that the metal orbitals of the{(I)(ttb-terpy)Ru}subunits are significantly higher in energy than those of the$\{(bpy)_2Ru\}$ subunits, due to the presence of the halide ligand(s).§ So, it could be expected that the metal-metal interaction increases on moving from **3** to **4**, contrary to the experimental results. The disagreement between indications derived from ΔV and expectation based on the energy gap of metal-centered and bridge-centered orbitals could suggest that the localized molecular orbital approximation, implicitly used for the superexchange theory as well as for the attribution of excited states in Ru(II) polypyridine complexes is not fully suited for the studied complexes, possibly because the oxidation process of **4** can involve a non-negligible contribution from iodide-based orbitals.†,[22] This in spite that the spectroscopic assignments used for the absorption spectra and the pump-probe experiments described above support the localized orbital approximation. However, reorganization energy connected to electron transfer can also have a role, and allows to reconciliate the apparent disagreement, as will be discussed later.

Table 3. Redox data of **1-4** in acetonitrile solution.

Coumpound	E(1/2)ox, V vs SCE	E(1/2)red, V vs SCE
Ru(bpy)3	1.27	-1.34,-1.52
1[a]	1.40	-0.63, -1.06, -1.59
2[b]	0.93, 1.52[c]	-0.44, -0.80
3[a]	1.34, 1.57[c]	-0.31, -0.67, -1.49
4	0.83, 1.01[c]	-0.53, -0.77

(a) Data from ref. 11. (b) Data from ref. 3d (c) Irreversible process. The reported value is the differential pulse volammetry peak.

We performed spectroelectrochemistry experiments on compounds **2, 3** and **4** in acetonitrile solution (supporting electrolyte: $[(CH_3CH_2CH_2CH_2)_4N(PF_6)]$ 0.05 M). The experiments were performed in an OTTLE cell, by applying a redox potential corresponding to the first oxidation process for each species.

Figure 7 shows the absorption spectral changes observed for **3** upon oxidation. A band appears between 8000 and 4500 cm^{-1}, with a maximum at 5700 cm^{-1}. On the basis of its shape (in particular, of its asymmetry), this band can be attributed to an intervalence charge transfer (IVCT) transition characterized by borderline Class II - Class III behavior.[23] The concomitant bleaching in the range 18000-12000 cm^{-1} is attributed to the partial disappearance of the spin-allowed MLCT transitions, due to the oxidation of one Ru(II) center.

Qualitatively similar behavior is observed for **2**. In the differential absorption spectral changes shown in **Figure 8**, it is possible to observe a very weak (see inset) band between 8500 and 4500 cm^{-1}. This less intense band is attributed to IVCT transitions. Unfortunately, the strong overlap of this band with the MLCT bleaching forbids to have information on the IVCT band shape and intensity. However, a borderline Class II/ Class III behavior is reasonable in this case, confirming that the localized nature of the MLCT states and levels is still acceptable, in spite of the significant interaction of the two metal centers via the bridging ligand. An apparently different scenario occurs for **4**. In fact, no net IVCT band appears in the 4000-10000 cm^{-1} range upon oxidation for this species (see **Figure 9**).

To better understand the differences in IVCT transitions in **2-4**, it is useful to recall that a commonly used relationship for the prediction of the energy maxima of intervalence transitions (ν_{max}) in dinuclear metal complexes is shown in eqn 1.[24]

$$\upsilon_{(max)} = \lambda_i + \lambda_0 + \Delta E_0 + \Delta E' \qquad \text{eqn. 1}$$

In such an equation, λ_i e λ_0 are the inner- and outer-sphere Franck–Condon reorganization contributions to the electron transfer barrier, respectively, ΔE_0 is the redox asymmetry factor (that is, $e\Delta V$, the separation between first and second oxidation potentials multiplied by the electron

charge), and ΔE' is the spin–orbit coupling contribution. We have estimated ν_{max} for compounds **2** and **3**, neglecting the λ_i and ΔE', and calculated λ_0 according to eqn 2.

$$\lambda_0 = e^2\left(\frac{1}{2R_a} + \frac{1}{2R_b} - \frac{1}{R_{ab}}\right)\left(\frac{1}{D_{op}} - \frac{1}{D_s}\right) \qquad \text{eqn. 2}$$

In eqn 2, R_a and R_b are the molecular radii, R_{ab} is the distance between the donor and acceptor, and D_{op} and D_s are the optical dielectric and static constants of the solvent, respectively.

By using equations 1 and 2, for complex **3** we obtained a ν_{max} value of 5600 cm^{-1}, in very good agreement with the experimental value (5700 cm^{-1}, see **Figure 7**), whereas for complex **2** the calculated ν_{max} value is 6800 cm^{-1}. In the latter case the experimental value of ν_{max} is impossible to be determinated, because of the strong overlap between the IVCT band and MLCT bleaching. However the tail of the experimental IVCT band (see **Figure 8**) would suggest some agreement with the calculation.[ß] For complex **4**, we have obtained a theoretical value of 2030 cm^{-1}, but this value is outside the instrumental limit, so the absence of any IVCT band in the studied spectral range (**Figure 9**) appears reasonable.[#]

The key to interpret the different ν_{max} calculated for **2-4** is to focus on the molecular radii of the {(I)(ttb-terpy)Ru(μ–dntpz)} and {$(bpy)_2$Ru(μ–dntpz} subunits. By the molecular CPK modelling of **2** and **3** and the X-ray analysis of **3**[3d] we calculated a molecular radius of 5.0 Å for the {$(bpy)_2$Ru(μ–dntpz} subunit and a radius of 6.10 Å for the {(I)(ttb-terpy)Ru(μ–dntpz)}$^+$ subunit. The calculated R_{ab} distance in **2-4** is 6.35 Å (as approximated by the metal-metal distance). The different molecular radii of the subunits are mainly due to the presence of the bulky *tert*-butyl substituents on the terpyridine ligand. This leads to quite different λ_0 reorganization energies for electron transfer. The calculated λ_0 are 5.9, 10.0, and 1.7 Kcal/mol for **2**, **3**, and **4**, respectively so that different ν_{max} values are obtained in spite of the relatively close eΔV values of the symmetric dinuclear species **3** and **4**. These results evidence the significant impact, sometimes underestimated, of the reorganization energy on the IVCT band energy. The different reorganization energies for electron transfer of the {(I)(ttb-terpy)Ru(μ–dntpz)} and {$(bpy)_2$Ru(μ–dntpz} subunits can

contribute to the experimentally small difference in ΔV between the first and second oxidation of **3** and **4**, which would suggest a small difference in the metal-metal interaction of the complexes depending on whether λ_o is disregarded (see redox discussion above). This observation confirms that for electronic interaction in dinuclear metal complexes, even in a rough approximation, the energy difference between orbitals involved in the virtual states is clearly important but cannot be used alone in estimating the extent of the interaction.

Finally, although it was not possible to perform pump-pulse ultrafast spectroscopy under photocatalytic conditions because the system is unstable under laser light, some points can be considered. Assuming that the excited-state processes are qualitatively similar in acetonitrile and aqueous solutions, it is immediately clear that the excited state of the $\{(I)(ttb\text{-}terpy)Ru(\mu\text{–}dntpz)\}^{+}$ catalytic subunit does not have enough energy to reduce persulfate and thus initiate the process. As a consequence, for **2** to be able to photo-drive water oxidation, as experimentally reported,[7] electron transfer to persulfate has to involve the chromophoric $\{(bpy)_2Ru(\mu\text{–}dntpz)\}^{2+}$ subunit. Such a process must compete with the very fast energy transfer process (170 fs in acetonitrile). So, the persulfate anion must be strongly ion-paired with the positively-charged complex at the ground state, a condition that is indeed quite common for highly-charged Ru(II) polypyridine complexes.[25] For regenerative DSPECs photoinjection into the TiO_2 semiconductor is also ultrafast[14,26] and can compete with fast intercomponent energy transfer, so compound **3** could be employed usefully. However, it would be more reasonable that the acceptor ligand of the lowest-energy MLCT state is a peripheral ligand directly connected with the semiconductor, maximizing electron coupling between chromophore and electrode. A different design of chromophore-catalyst dyads is therefore to be preferred.

Conclusions

The early photophysical events occurring in the chromophore-catalytic molecular dyad **2**, as well as in its model species **1, 3**, and **4,** have been studied. For completeness, the absorption spectra and redox behavior of **1-4** and the spectroelectrochemistry of the dinuclear **2-4** species have also been investigated. In **2**, energy transfer from the MLCT state involving the chromophoric $\{(bpy)_2Ru(\mu\text{–}dntpz)\}^{2+}$ unit to the MLCT level involving the catalytic $\{(I)(ttb\text{-}terpy)Ru(\mu\text{–}dntpz)\}^{+}$ unit takes place with a time constant of 170 fs (rate constant, 5.9 x 10^{12} s^{-1}). The energy transfer process is followed by a charge redistribution in the excited state possibly coupled with some structural reorganization, with a time constant of 2.5 ps, and finally by decay to the ground state, assisted by thermal activation to a low-lying MC state involving the $\{(I)(ttb\text{-}terpy)Ru(\mu\text{–}dntpz)\}^{+}$ unit, with a time constant of 25 ps. Noteworthy, the inter-component energy transfer in **2** and the thermally-assisted MLCT-to-MC activation process in **2** and **4** occur on timescales that are mostly shorter than the MLCT vibrational cooling as recorded in **1** and **3**. This indicates that both intercomponent energy transfer and MLCT-to-MC activation process take place from non-equilibrated MLCT states.

Redox data and spectroelectrochemistry experiments suggest that **2-4** behave as borderline Class II/Class III species as far as the metal-metal electronic interaction is concerned. The absence of a net IVCT band of the mono-oxidized **4** at energies higher than 4000 cm^{-1} compares to the net IVCT band shown by the mono-oxidized **3** at about 5700 cm^{-1}. The results evidence the importance of the reorganization energy for electron transfer in determining the energy of the IVCT band in dinuclear Ru(II) polypyridine complexes.

Acknowledgements

We thank Franco Scandola for helpful suggestions on the spectroelectrochemistry section. RT thanks the U.S. Department of Energy, Office of Science, Office of Basic Energy Sciences under award no. DE-FG02-07ER15888 and the Robert A. Welch Foundation (E-621). A fellowship grant

(Ministero degli Affari Esteri e della Cooperazione Internazionale, MAECI) to AS is also acknowledged.

Electronic Supplementary Information

Electronic supplementary information (ESI) available: General procedures, equipments and methods, synthesis and characterization details.

References and notes

¶ Electron hopping in $[Ru(bpy)_3]^{2+}$ occurs in a few ps,[13] so processes with a large driving force should be much faster. However, conversion between the two low-lying MLCT states cannot be totally ruled out as being responsible for the fast decay process in **1**.

§ As a second order effect, even the bridging ligand orbitals are higher in energy in **4** than in **3**, but to a minor extent. In fact, the difference in the first oxidation potential between **3** and **4** is 510 mV, whereas the difference in the reduction potential is 220 mV (see **Table 2**). So, the effect of the presence on halide ligands on the bridge orbitals is not enough to counterbalance the effect on the metal-based orbitals.

† In fact, the HOMO of the somewhat related compound $[Ru(bpy)(terpy)Cl]^+$ consists mainly of an antibonding combination of a t_{2g} orbital on the metal and a p orbital on the chloride ligand, according to a DFT calculation in acetone, dichloromethane, water and in vacuum. See ref. 22.

¢ A less intense bleaching is also present in the 8000-10000 cm^{-1} range, also visible for **2** and **4** (see later; for **2**, where the bleaching is not overlapped with an IVCT band, the bleaching extends towards 6000 cm^{-1}). Such a low-energy bleaching is assigned to the disappearance of spin-forbidden MLCT bands.

ß In fact, **Figure 8** suggests that for **2**, ν_{max} could be at higher energy than 8000 cm^{-1}. This could be a consequence of the nature of the oxidation process for the $\{(I)(ttb\text{-}terpy)Ru(\mu\text{–}dntpz)\}^+$ subunit, which can involve contribution from the iodide ligand (see ref. 22 and note †), so the R_{ab} donor-acceptor distance in eqn. 2 would be larger than the metal-metal separation in **2**. The mixed origin (Ru-I) of the donor orbital of the IVCT band in **2** could also justify the extremely low intensity of such a band, in comparison with the IVCT band of **3** (compare **Figures 7** and **8**).

According to what is discussed in note ß, the ν_{max} for **4** could be at higher energy than the calculated value of 2030 cm^{-1}, but probably lower than our instrumental limit of 4000 cm^{-1}.

(1) The topic is too vaste to be exhaustively quoted. For some representative articles, see: (a) J. H. Alstrum-Acevedo, M. K. Brennaman and T. J. Meyer, *Inorg. Chem.*, 2005, **44**, 6802. (b) R. Zong and R. P. Thummel, *J. Am. Chem. Soc.*, 2005, **127**, 12802. (c) I. Romero, M. Rodriguez, C. Sens, J. Mola, M. R. Kollipara, L. Francis, E. Mas-Marza, L. Escriche and A. Llobet, *Inorg. Chem.*, 2008, **47**. 1824. (d) J. J. Concepcion, J. W. Jurss, J. L. Templeton and T. J. Meyer, *J. Am. Chem. Soc.* 2008, **130**, 16462. (e) F. Liu, J. J. Concepcion, J. W. Jurss, T. Cardolaccia, J. L. Templeton and T. J. Meyer, *Inorg. Chem.*, 2008, **47**, 1727. (f) H.W. Tseng, R. Zong, J. T. Muckerman, R. Thummel, *Inorg. Chem*., 2008, **47**, 11763. (g) J. J. Concepcion, J. W. Jurss, J. L. Templeton and T. J. Meyer, *J. Am. Chem. Soc.*, 2008, **130**, 16462. (h) A. Sartorel, M. Carraro, G. Scorrano, R. De Zorzi, S. Geremia, N.D. McDaniel, S. Bernhard, M. Bonchio, *J. Am. Chem. Soc.*, 2008, **130**, 5006. (i) H. Yamazaki, A. Shouji, M. Kajita and M. Yagi, *Coord. Chem. Rev.*, 2010, **254**, 2483. (j) S. Roeser, M. Z. Ertem, C. Cady, R. Lomoth, J. Benet-Buchholz, L. Hammarstroem, B. Sarkar, W. Kaim, C. J. Cramer, A. Llobet, *Inorg. Chem.* 2012, **51**, 320.

(2) (a) S. W. Gersten, G. J. Samuels and T. J. Meyer, *J. Am. Chem. Soc.,* 1982, **104**, 4029. (b) J. A. Gilbert, D. S. Eggleston, W. R. Murphy, D. A. Geselowitz, S. W. Gersten, D. J. Hodgson and T. J. Meyer, *J. Am. Chem. Soc.*, 1985, **107**, 3855.

(3) See, for example: (a) L. Duan, F. Bozoglian, S. Mandal, B. Stewart, T. Privalov, A. Llobet and L. Sun, *Nat. Chem.*, 2012, **4**, 418. (b) S. Maji, L. Vigara, F. Cottone, F. Bozoglian, J. Benet-Bichholz and A, Llobet, *Angew. Chem. Int. Ed.*, 2012, **51**, 5967. (c) D. Moonshiram, I. Alperovich, J. J. Concepcion, T. J. Meyer and Y. Pushkar, *Proc. Natl. Acad. Sci. U. S. A.*, 2013, **110**,3765. (d) L. Kohler, N. Kaveevivitchai, R. Zong, and R. P. Thummel *Inorg. Chem*. 2014, **53**, 912. (e) J. D. Blackmore, R. H. Crabtree and G. W. Brudvig, *Chem. Rev.*, 2015, **115**, 12974. (f) L. Tong and R. P. Thummel, *Che. Sci.*, 2016, **7**, 6591. (g) Y. Tsubonouchi, S. Lin, A. R. Parent, G. W. Brudvig and K. Sakai, *Chem. Commun.*, 2016, **52**, 8018. (h) T. J. Meyer,

M. W. Sheridan and B. D. Sherman, *Chem. Soc. Rev.*, 2017, **46**, 6148. (i) G. W. Brudvig, S. Campagna, *Chem. Soc. Rev.*, 2017, **46**, 6085. (j) D. W. Shaffer, Y. Xie and J. J. Concepcion, *Chem. Soc. Rev.*, 2017, **46**, 6170.

(4) (a) J. J. Concepcion, M.-K. Tsai, J. T. Muckerman and T. J. Meyer, *J. Am. Chem. Soc.*, 2010, **132**, 1545. (b) D. E. Polyansky, J. T. Muckerman, J. Rochford, R. Zong, R. P. Thummel and E. Fujita, *J. Am. Chem. Soc.*, 2011, **133**, 14665. (c) A. Lewandowska-Andralojc, D. E. Polyansky, R. Zong, R. P. Thummel and E. Fujita, *Phys. Chem. Chem. Phys.*, 2013, **15**, 14058. (d) R. Matheu, M. Z. Ertem, J. Benet-Buchholz, E. Coronado, V. S. Batista, X. Sala and A. Llobet, *J. Am. Chem. Soc.*, 2015, **137**, 10786.

(5) (a) L. Duan, L. Wang, A. K. Inge, A. Fisher, X. Zou and L. Sun, *Inorg. Chem.*, 2013, **52**, 7844 (b) D. W. Shaffer, Y. Xie, D. J. Szalda and J. J. Concepcion, *Inorg. Chem.*, 2016, **55**, 12024. (c) T. Fan, L. Duan, P. Huang, H. Chen, Q. Daniel, M. S. G. Ahlqyuist and L. Sun, *ACS Catal.*, 2017, **7**, 2956. (d) Y. Xie, D. W. Shaffer and J. J. Concepcion, *Inorg. Chem.*, 2018, **57**, 10533, and refs. therein.

(6) (a) C. J. Richmond, R. Matheu, A. Poater, L. Falivene, J. Benet-Buchholz, X. Sala, L. Caballo and A. Llobet, *Chem. Eur. J.*, 2014, **20**, 17282. (b) D. L. Ashford, M. K. Gish, A. K. Vannucci, M. K. Brennaman, J. L. Templeton, J. M. Papanikolas and T. J. Meyer, *Chem. Rev.*, 2015, **115**, 13006, and refs. therein.

(7) N. Kaveevivitchai, R. Chitta, R. Zong, M. El Ojaimi and R. P. Thummel, *J. Am. Chem. Soc.*, 2012, **134**, 10721.

(8) (a) M. K. Brennaman, R. J. Dillon, L. Alibabaei, M. K. Gish, C. J. Dares, D. L. Ashford, R. L. House, G. J. Meyer, J. M. Papanikolas and T. J. Meyer, *J. Am. Chem. Soc.*, 2016, **138**, 13085. (b) B. D. Sherman, Y. Xie, M. V. Sheridan, D. Wang, D. W. Shaffer, T. J. Meyer, and J. J. Concepcion, *ACS Energy Lett.*, 2017, **2**, 124. (c) B. Shan, B. D. Sherman, C. M. Klug, A. Nayak, S. L. Marquard, Q. Liu, R. M. Bullock and T. J. Meyer, *J. Phys. Chem. Lett.*, 2017, **8**,

4374. (d) B. Shan, A. Nayak, M. K. Brennaman, M. Liu, S. L. Marquard, M. S. Eberhart and T. J. Meyer, *J. Am. Chem. Soc.*, 2018, **140**, 6493. (e) L. Wu, M. Eberhart, A. Nayak, M. K. Brennaman, B. Shan and T. J. Meyer, *J. Am. Chem. Soc.*, Article ASAP, DOI: 10.1021/jacs.8b10132.

(9) J. T. Hewitt, J. J. Concepcion and N. H. Damrauer, *J. Am. Chem. Soc.*, 2013, **135**, 12500.

(10) M. Chrzanowska, A. Katafias, O. Impert, A. Kozakiewicz, A. Surdykowski, P. Brzozowska, A. Zachl, R. Puchta and R. van Eldik, *Dalton Trans.*, 2017, **46**, 10264, and refs therein.

(11) D. Brown, S. Muranjan, and R. P. Thummel *Eur. J. Inorg. Chem.* **2003**, 3547.

(12) J. M. McCusker, *Acc. Chem. Res.*, 2003, **36**, 876. (b) M. Chergui, *Acc. Chem. Res.*, 2015, **49**, 801 and refs. therein.

(13) (a) S. Campagna, F. Puntoriero, F. Nastasi, G. Bergamini and V. Balzani, *Top. Curr. Chem.*, 2007, **280**, 117, and refs. therein.

(14) Vibrational cooling in the same time range have been reported for several transition metal polypyridine complexes, see for example: (a) A. El Nahhas, C. Consanti, A. M. Blanco-Rodriguez, K. M. Lancaster, O. Braem, A. Cannizzo, M. Towrie, I. Clarck, S. Zalis, M. Chergui and A. Vlcek, *Inorg. Chem.*, 2011, **50**, 2932. (b) F. Nastasi, F. Puntoriero, M. Natali, M. Mba, M. Maggini, P. Mussini, M. Panigati and S. Campagna, *Photochem. Photobiol. Sci.*, 2015, **14**, 909.

(15) F. Puntoriero, F. Nastasi, M. Galletta and S. Campagna, In *Comprehensive Inorganic Chemistry* II (Eds.: J. Reedijk, K. Poeppelmeier), Vol. 8, Oxford: Elsevier, 2013, pp. 255-337.

(16) (a) T. J. Meyer, *Pure Appl. Chem.*, 1986, **58**, 1193, and refs. therein. (b) A. Juris, V. Balzani, F. Barigelletti, S. Campagna, P. Belser and A. von Zelewsky; *Coord. Chem. Rev.*, 1988, **84**, 85.

(17) (a) H. Berglund Baudin, J. Davidsson, S. Serroni, A. Juris, V. Balzani, S. Campagna and L. Hammarström, *J. Phys. Chem. A*, 2002, **106**, 4312. (b) J. Andersson, F. Puntoriero, S. Serroni,

A. Yartsev, T. Pascher, T. Polivka, S. Campagna and V. Sundström, *Chem. Phys. Lett.*, 2004, **386**, 336. (c) J. Andersson, F. Puntoriero, S. Serroni, A. Yartsev, T. Pascher, T. Polivka, S. Campagna and V. Sundström, *Faraday Discussions*, 2004, **127**, 295. (d) J. Larsen, F. Puntoriero, T. Pascher, N. McClenaghan, S. Campagna, E. Åkesson and V. Sundström, *ChemPhysChem*, 2007, **8**, 2643.

(18) (a) G. Denti, S. Campagna, L. Sabatino, S. Serroni, M. Ciano and V. Balzani, *Inorg. Chem.,* 1990, **29**, 4750. (b) A. Arrigo, G. La Ganga, F. Nastasi, S. Serroni, A. Santoro, M.-P. Santoni, M. Galletta, S. Campagna and F. Puntoriero, *C. R. Chimie*, 2017, **20**, 209.

(19) (a) G. Giuffrida and S. Campagna, *Coord. Chem. Rev.*, 1994, **135-136**, 517. (b) M. D. Ward, *Chem. Soc. Rev.* 1995*,* **24**, 121 and refs. therein.

(20) M. Natali, S. Campagna and F. Scandola, *Chem. Soc. Rev.,* 2014**, 43***,* 4005.

(21) T.Koopmans, *Physica,* 1934*,* **1**, 104.

(22) E. Jakubikova, W. Chen, D. N. Dattelbaum, F. N. Rein, R. C. Rocha, R. L. Martin and E. R. Batista, *Inorg. Chem.*, 2009, **48,** 10720.

(23) B. S. Brunschwig, C. Creutz and N. Sutin, *Chem. Soc. Rev.*, 2002, **31**, 168 and refs. therein.

(24) D. M. D'Alessandro, F. R. Keane, *Chem. Soc. Rev.*, 2006, **35**i, 424.

(25) (a) M. Burian, Z. Syrgiannis, G. La Ganga, F. Puntoriero, M. Natali, F. Scandola, S. Campagna, M. Prato, M. Bonchio, H. Amenitsch and A. Sartorel, *Inorg. Chim. Acta*, 2017, **454**, 171. (b) A. Arrigo, F. Puntoriero, G. La Ganga, S. Campagna, M. Burian, S. Bernstorff and H. Amenitsch, *Chem*, 2017, **3**, 494.

(26) (a) J. E. Moser and M. Graetzel, *Chem. Phys.*, 1993, **176**, 493. (b) Y. Tachibana, J. E. Moser, M. Grätzel, D. R. Klug and J. R. Durrant, *Chem. Phys. Lett.*, 1997, **272**, 489. (c) N. S. McCool, J. R. Swierk, C. T. Nemes, C. A. Schmuttenmaer and T. E. Mallouk, *J. Phys. Chem. Lett.*, 2016, **7**, 2930. (d) J. R. Swierk, N. S. McCool, C. T. Nemes, T. E. Mallouk and C. A.

Schmuttenmaer, *J. Phys. Chem. C*, 2016, **120**, 5940. (e) C. S. Ponseca, P. Chabera, J. Uhlig, P. Persson and V. Sundstroem, *Chem. Rev.*, 2017, **117**, 10940.

Figures and captions

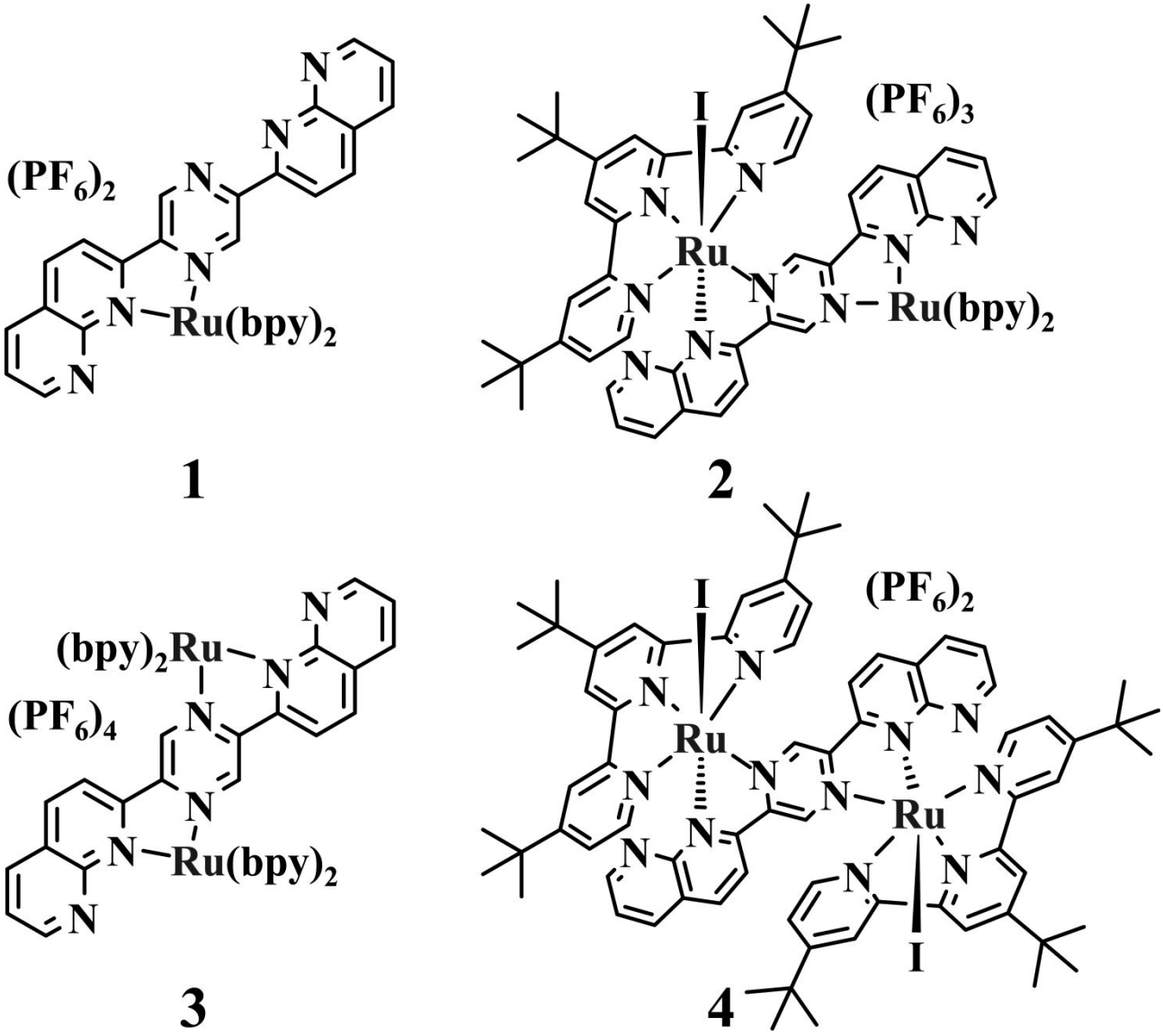

Figure 1. Structural formulae of **1-4**.

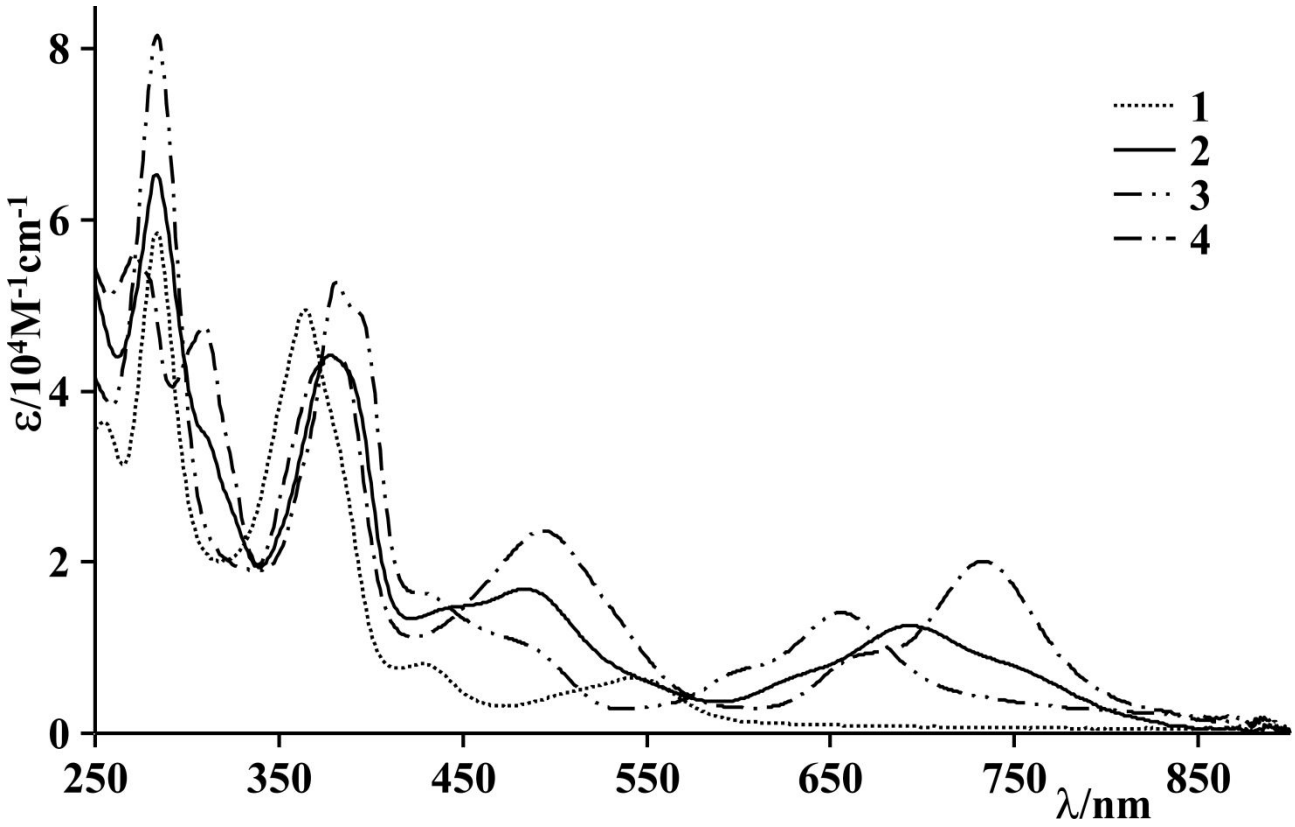

Figure 2. Absorption spectra of **1-4** in acetonitrile solution.

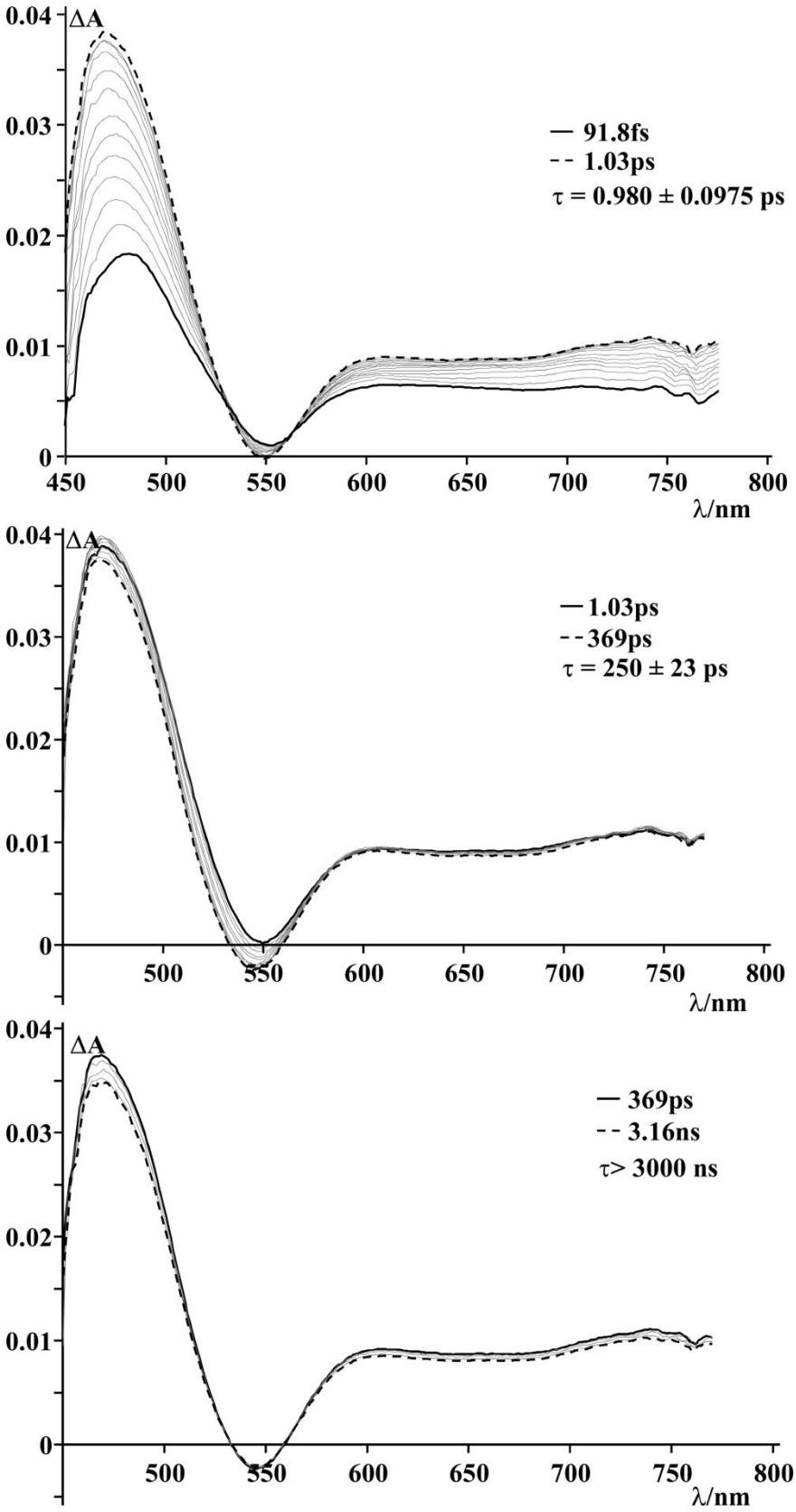

Figure 3. Transient absorption spectra of **1** in acetonitrile, recorded at different delay times. Excitation wavelength, 400 nm. Time constants of the various processes are also reported in the Figure.

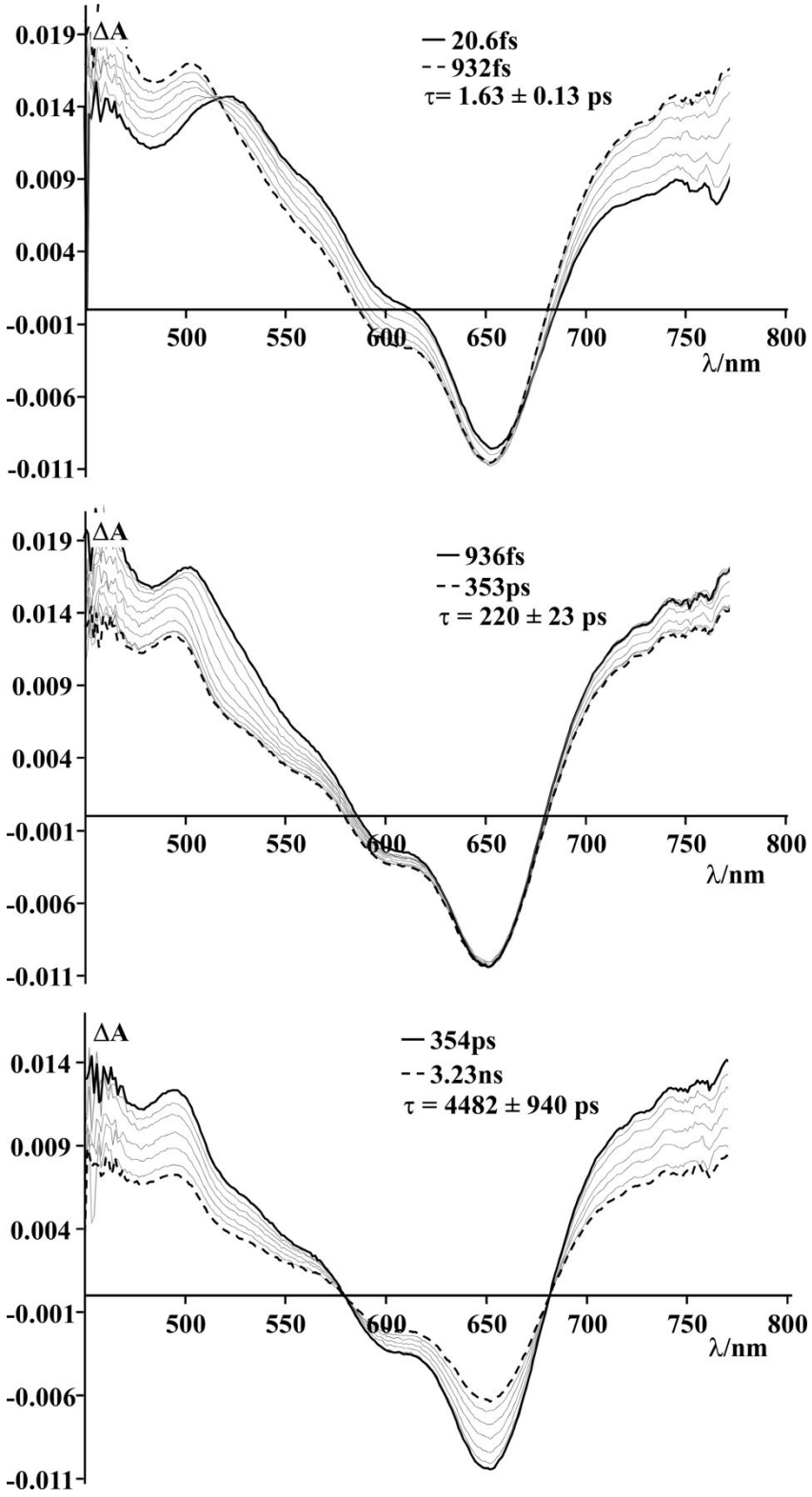

Figure 4. Transient absorption spectra of **3** in acetonitrile, recorded at different delay times. Excitation wavelength, 400 nm. Time constants of the various processes are also reported in the Figure.

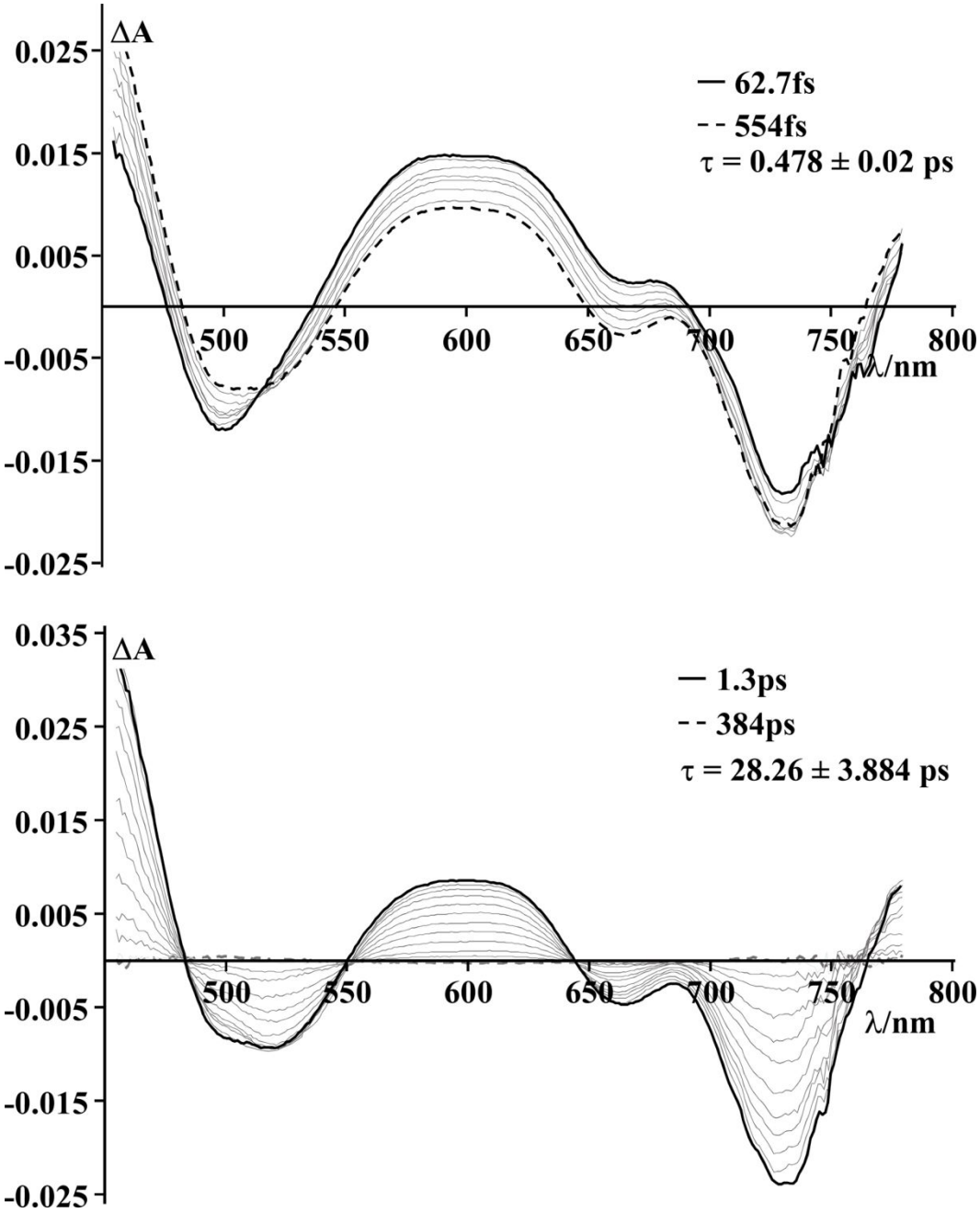

Figure 5. Transient absorption spectra of **4** in acetonitrile, recorded at different delay times. Excitation wavelength, 400 nm. Time constants of the various processes are also reported in the Figure.

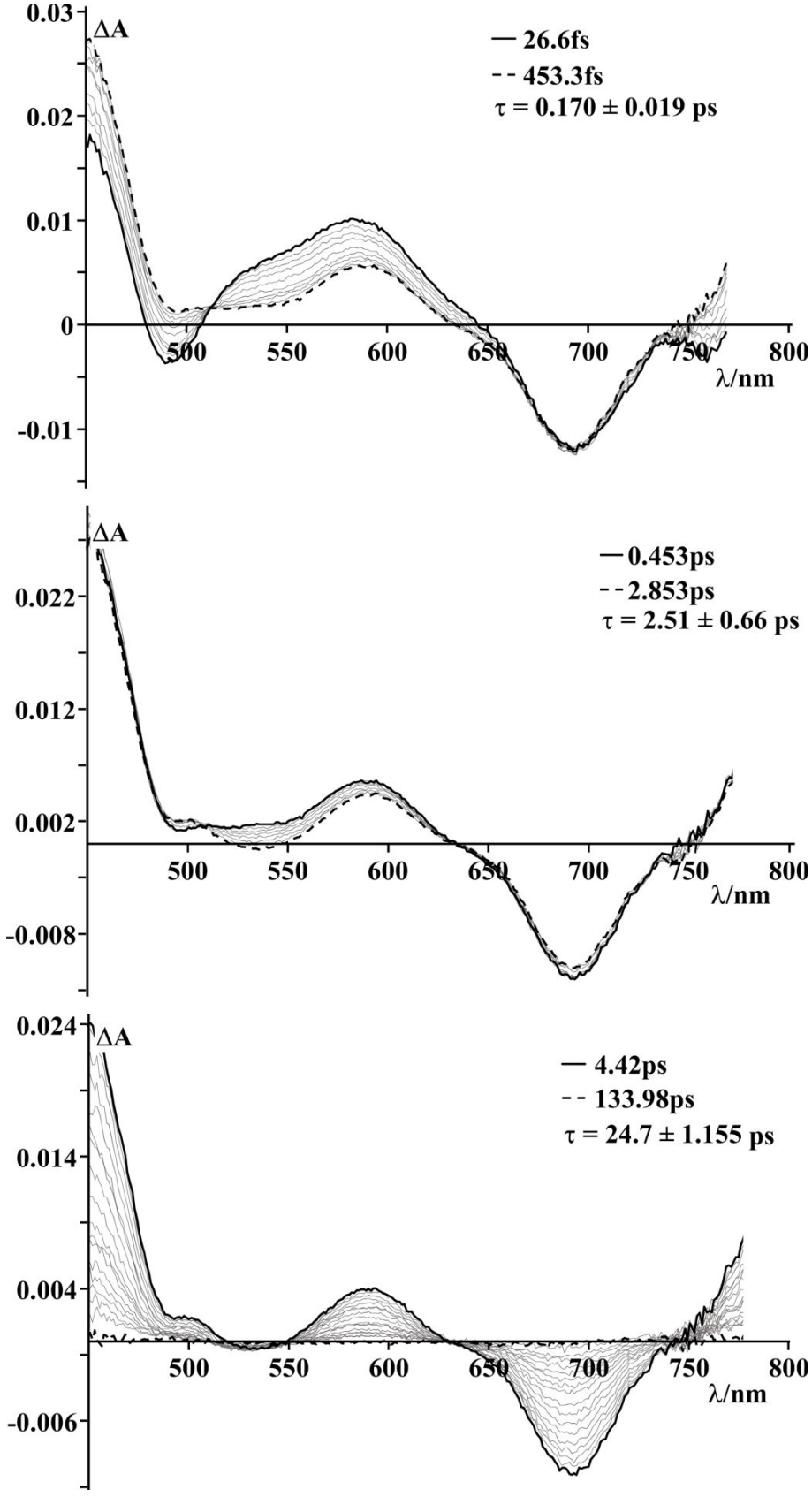

Figure 6. Transient absorption spectra of **2** in acetonitrile, recorded at different delay times. Excitation wavelength, 400 nm. Time constants of the various processes are also reported in the Figure.

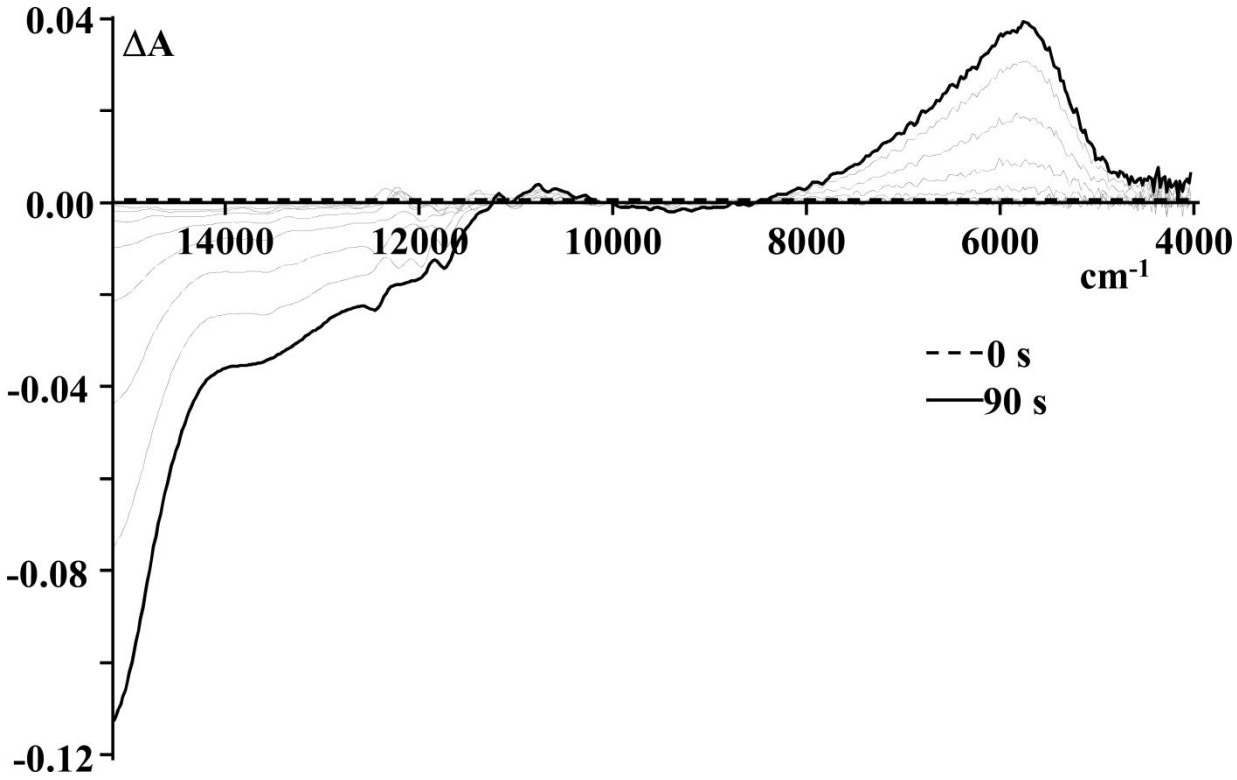

Figure 7: Differential spectrum between the absorption spectra of the oxidized and ground states of **3** upon first oxidation (1.04×10^{-3} M, acetonitrile solution). The applied potential is 1.38 V *vs* SCE.

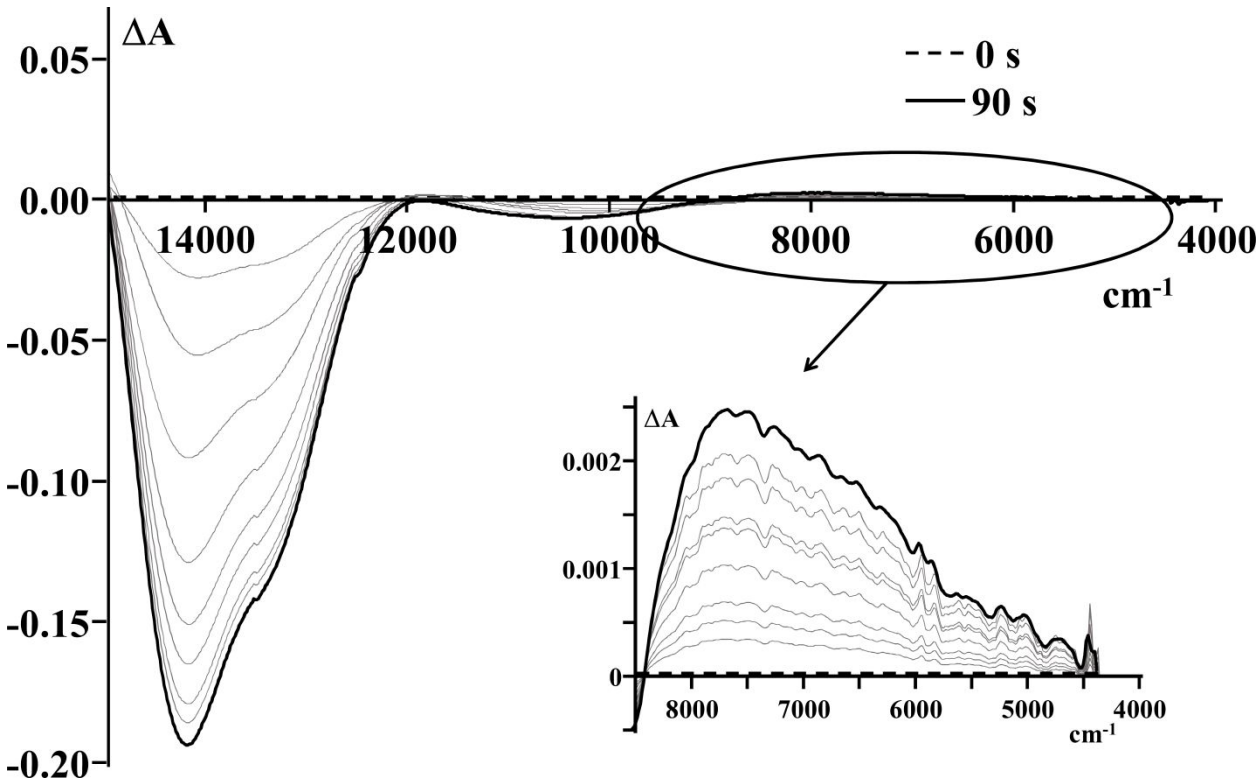

Figure 8: Differential spectrum between absorption spectra of the oxidized and ground states upon the first oxidation of **2** (2.08×10^{-3} M, acetonitrile solution). The applied potential is 0.90 V *vs* SCE.

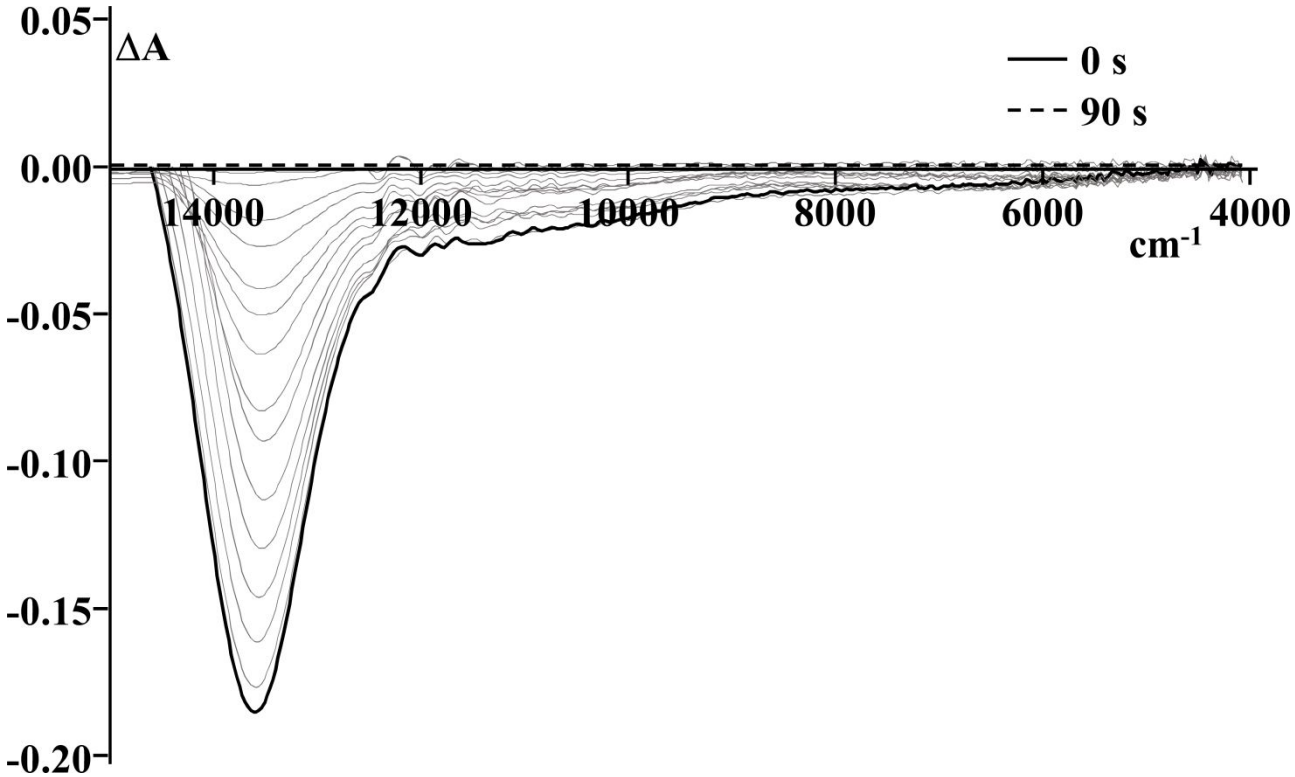

Figure 9. Differential spectrum between absorption spectra of the oxidized and ground states upon the first oxidation of **4** (3.84×10^{-4} M, acetonitrile). The applied potential is 0.83 V *vs* SCE.

Graphical abstracts

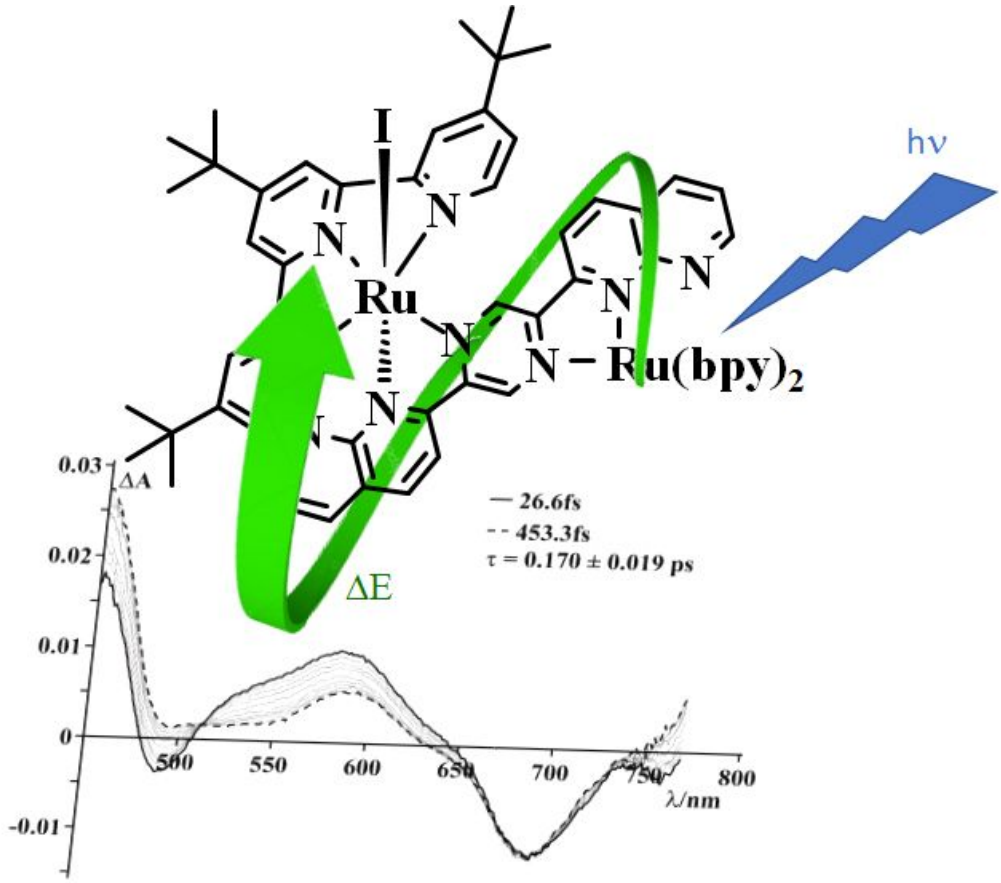

Early events in a water oxidation chromophore-catalyst species are studied; ultrafast energy transfer occurs from the chromophore to the catalytic unit